frontiers in Marine Science

ORIGINAL RESEARCH
published: 29 July 2021
doi: 10.3389/fmars.2021.694614

The Norwegian Sea Gyre – A Regulator of Iceland-Scotland Ridge Exchanges

Hjálmar Hátún[1], Léon Chafik[2] and Karin Margretha Húsgarð Larsen[1]*

[1] Faroe Marine Research Institute, Tórshavn, Faroe Islands, [2] Department of Meteorology and Bolin Centre for Climate Research, Stockholm University, Stockholm, Sweden

The Norwegian Sea gyre (NSG) is a large body of Arctic intermediate water and deep dense overflow waters, which circulate counterclockwise within the Norwegian Sea. Argo float trajectories presented in this study suggest that the NSG attains its strongest and most focused flow downstream of a confluence of subarctic waters from the Iceland Sea and the Jan Mayen Ridge at steep bathymetry north of the Faroe slope. Based on hydrographic data from a meridional standard section across this flow (1988 to present), the first baroclinic estimate of the NSG circulation strength is provided. We, furthermore, show that the NSG circulation regulates key aspects of both the poleward Atlantic Water (AW) currents and the equatorward near-bottom and mid-depth flows in the Norwegian Sea – the main arteries of the Meridional Overturning Circulation. More specifically, we demonstrate close links between the NSG circulation and (i) the observed Faroe Bank Channel Overflow (FBCO) transport, (ii) variable depth of the main thermocline separating AW from the underlying colder and denser subarctic water masses, and (iii) satellite-derived sea-surface heights (SSHs) in the southern Nordic Seas. In general, a strong NSG and weak FBCO transport are associated with an uplifted thermocline and depressed SSH. Along a narrow band near the Norwegian and Shetland slopes, a strong NSG – oppositely – links to a depressed interface. Daily records of the FBCO transport, and satellite altimetry in a sensitive region north of the Iceland-Faroe Ridge, complement our hydrographic monitoring of the NSG strength. Together these records constitute valuable indicators for aspects of the Norwegian Sea physical oceanography, which likely have an impact on regional climate, ecology and biological productivity.

Keywords: overflow, Atlantic inflows, main thermocline, Norwegian Sea Gyre, ecological indicator

OPEN ACCESS

Edited by:
Benjamin Rabe, Alfred Wegener Institute, Helmholtz Centre for Polar and Marine Research (AWI), Germany

Reviewed by:
Andreas Macrander, Marine and Freshwater Research Institute, Iceland
Robert Pickart, Woods Hole Oceanographic Institution, United States

****Correspondence:***
Hjálmar Hátún
hjalmarh@hav.fo

Specialty section:
This article was submitted to Physical Oceanography, a section of the journal Frontiers in Marine Science

Received: *13 April 2021*
Accepted: *02 July 2021*
Published: *29 July 2021*

Citation:
Hátún H, Chafik L and Larsen KMH (2021) The Norwegian Sea Gyre – A Regulator of Iceland-Scotland Ridge Exchanges. Front. Mar. Sci. 8:694614. doi: 10.3389/fmars.2021.694614

INTRODUCTION

Total volume and heat transports from the North Atlantic to the Nordic Seas are estimated from observations along monitoring arrays at the Greenland-Scotland Ridge (Hansen and Østerhus, 2000; Hansen et al., 2015). Whether these heat anomalies actually reach the high Arctic is, however, strongly determined by the flow dynamics within the Nordic Seas – especially in the eastern part. Realistic prediction of such anomalies in model systems requires proper representation of critical regional oceanic processes.

In the northeastern Atlantic, variable eastward extent and circulation intensity of the subpolar gyre (SPG – abbreviations are provided in **Table 1** and **Figure 1**) determines the relative contribution of Atlantic and subarctic source water masses to the resulting Modified North Atlantic Water (MNAW, and here referred to as just AW – **Table 2**), which subsequently feeds the Atlantic inflows toward the Arctic (Hátún et al., 2005a). AW enters the Nordic Seas as a new source water mass, where it interacts with the subarctic water masses of the Norwegian Sea Gyre (NSG; **Figure 1**), producing even more modified waters in this region (Read and Pollard, 1992). Source AW also enters the Nordic Seas through the Faroe-Shetland Channel, where it encounters a limb of the NSG extending into this channel (Hátún, 2004; Hansen et al., 2017; **Figure 1**). In this way, AW flows cyclonically around the southeastern Norwegian Sea, wedged between the continental slopes [north of the Iceland-Faroe Ridge (IFR), Faroe Plateau and west of Norway] and the body of the NSG.

Although the NSG is less flexible for lateral shifts compared to the SPG, its southward and eastward extent does also shift. As such, we here hypothesize that the NSG is a regulator of the main water masses in the southeastern Nordic Seas. That is, the NSG might play a mediating role within the Nordic Seas, comparable to the SPG regulation of the oceanography in the northeastern North Atlantic (Hátún et al., 2005a; Hátún and Chafik, 2018).

Variable westward AW extent is synonymous with the zonal position of the subarctic front in the eastern Norwegian Basin, and this issue has been observed and discussed over decades (Blindheim et al., 2000; Mork and Blindheim, 2000). The dynamics of this subarctic front – which north of the Faroes is called the Iceland-Faroe front – is directly linked to undulations in the main thermocline between the warm AW and the underlying subarctic water masse. This *interface*, as it hereafter will be referred to, is suggested to respond to the large-scale wind field, i.e., the North Atlantic Oscillation (NAO). Weak/strong NAO periods (denoted NAO− and NAO+, respectively) lead depressed/uplifted states, respectively, of the interface along the Faroe and Norwegian slopes (Mork and Blindheim, 2000; Richter and Maus, 2011).

Using a two-layer reduced gravity model, Orvik (2004) proposed a link between the flow directionality of the lower layer and the width and depth of the AW wedge. More specifically, he pointed out that when the deep topographically steered flow follows (opposes) that of the AW, the wedge area is reduced (expanded) and the interface separating the two main water masses deepens (shoals) as a result of a convergence (divergence) of AW locally. The link between the wind forcing in the Nordic Seas, the AW width and the interface depth must therefore involve changes in the deep currents.

Deep waters from the NSG and/or its immediate surroundings are funneled out through the narrow Faroe Bank Channel (FBC; **Figure 1**), and continuous observations of the Faroe Bank Channel Overflow (FBCO) transport are available since the mid-1990s (Hansen et al., 2016). Model experiments (Köhl, 2010; Serra et al., 2010) and a recent study combining both a high-resolution ocean general circulation model and observations from multiple platforms (Chafik et al., 2020) show that the FBCO is fed *via* two pathways – a western source from along the Faroe slope and an eastern source along the Norwegian slope region. Both branches converge into the newly discovered southwestward directed deep Faroe-Shetland Channel jet (FSCJ), located at the base of the Shetland slope (Chafik et al., 2020; **Figure 1**), before feeding the FBCO.

These three key aspects of the Norwegian Sea – the NSG, the interface depth and the FBCO – have all previously been separately linked to changes in sea-surface height (SSH). A wind-driven barotropic model by Nøst and Isachsen (2003) suggests a close link between the deep NSG-related flow and the SSH over the central Norwegian Sea. The most pronounced SSH variability is, however, observed over the AW wedge in the southeastern Norwegian Sea (Richter et al., 2012). It has been linked to undulations of the interface and to the hydrographic properties (density) of the AW – both through the steric relation (Siegismund et al., 2007; Richter et al., 2012). Variability in the FBCO is shown to correlate with the simulated SSH in the central Norwegian Basin (Olsen et al., 2008), and with satellite altimetry data integrated over a broad region farther north (Bringedal et al., 2018). It is, however, not clear where the most plausible drivers of FBCO variability (pressure, interface height, and SSH) have their center-of-action.

Since only water associated with the boundary current around the Norwegian basin can be in direct contact with the FBCO (Yang and Pratt, 2013) direct causal linkages between the overflow and SSH must be found within a bottom depth range comparable to the FBC sill depth (840 m).

The FBCO is likely driven by the southward pressure gradient between the Norwegian Sea and the northeast Atlantic pressure at the FBC sill depth (Olsen et al., 2008). This is, in turn, regulated by the height of the interface above the sill depth. Model studies confirm this expected link between stronger FBCO and a higher upstream interface (Sandø et al., 2012), but this link is only identifiable to the Shetland slope, and thus to the overflow-feeding FSCJ (Chafik et al., 2020). Also based on adjoint sensitivity calculations (a tool that helps to determine mechanisms of a chosen variable), Köhl, 2010 used the sensitivities $\partial \mathrm{FBCO}/\partial h_{27.8}$ to describe at which location perturbations of the local height of the $\sigma_\theta = 27.8$ surface ($h_{27.8}$) changes the FBCO most. This analysis showed that the interface height just north of the IFR is particularly sensitive to the FBCO transport variability (Köhl, 2010, their Figure 11B). This "negative sensitivity" between the overflow and the interface came as a surprise to these authors, who

TABLE 1 | List of abbreviations, arranged in alphabetical order.

Acronym	Name
FBCO	Faroe Bank Channel Overflow
FSCJ	Faroe-Shetland Channel Jet
IFSJ	Iceland-Faroe Slope Jet
NAO	North Atlantic Oscillation
NSG	Norwegian Sea Gyre
SPG	Subpolar Gyre
SSH	Sea-surface height

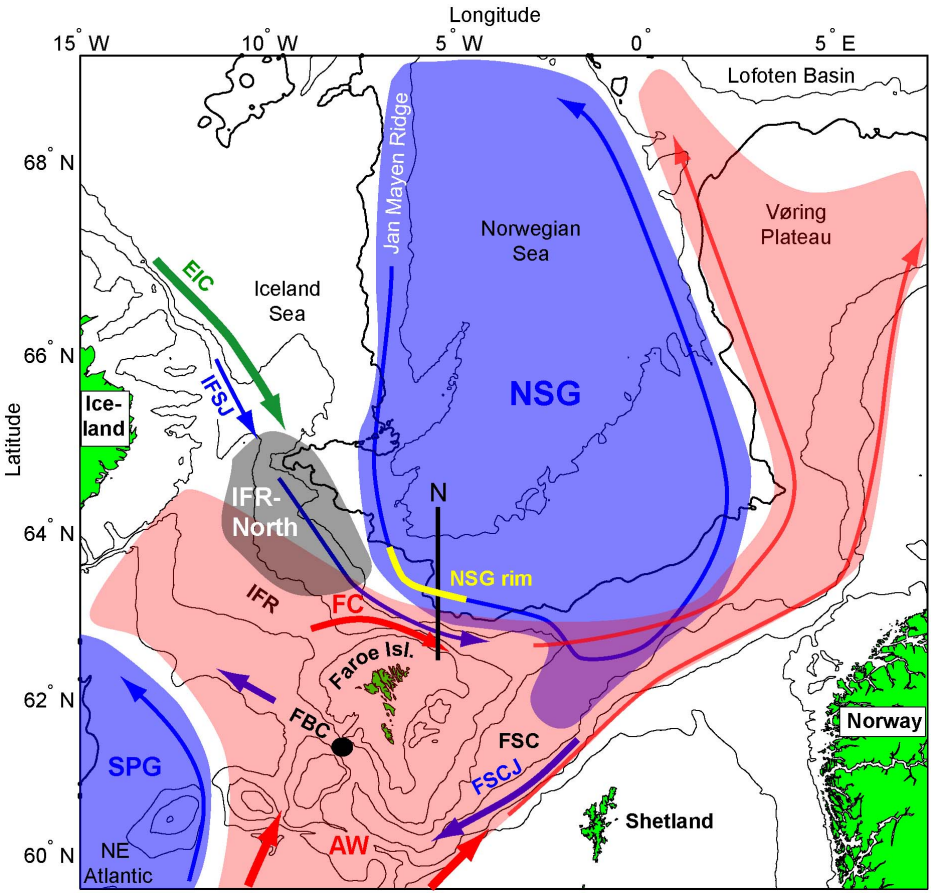

FIGURE 1 | Overview over the study region. The counterclockwise circulating Norwegian Sea Gyre (NSG) and the subpolar gyre (SPG) – composed of cold and dense subarctic waters – are highlighted in blue color. The *NSG rim* is outlined in yellow color and the IFR-North region is illustrated in gray. Poleward flowing AW are shown in red. The location of monitoring Section N is illustrated with a black line. FBC, Faroe Bank Channel; IFR, Iceland-Faroe Ridge; FSC, Faroe-Shetland Channel; FSCJ, Faroe-Shetland Channel Jet; IFSJ, Iceland-Faroe Slope Jet; FC, Faroe Current; and EIC, East Icelandic Current. The following depth contours are plotted: 200, 500, 1000, 2000 (heavy contour line), and 3000 m.

TABLE 2 | List of water mass abbreviations.

Acronym	Name	Temperature range	Salinity range
(MN)AW	(Modified North) Atlantic Water	>7°C	35.00 → 35.35
MEIW	Modified East Icelandic Water	1 → 3°C	<34.90
NNAW	Norwegian North Atlantic Water	2.5 → 3.2°C	34.96 → 34.99
NSAIW	Norwegian Sea Arctic Intermediate Water	−0.5 → 0.5°C	34.87 → 34.91
NSDW	Norwegian Sea Deep Water	<−0.5°C	34.90 → 34.92

could not provide a satisfactory explanation thereof. The present article presents a possible explanation of this apparent conundrum (see section "Contrasting NSG+/NSG− States and Possible Drivers").

Direct observations of the NSG intensity are not available, and only general aspects of this gyre system have been illustrated, e.g., using Lagrangian data sources – Argo floats (Voet et al., 2010), RAFOS floats (Søiland et al., 2008), and surface drifters (Jakobsen, 2003). Spatial structures are, however, lost in such studies due to the mapping of data onto relatively coarse grids. The idealized model by Nøst and Isachsen (2003) predicts strong bottom-intensified flows where the seabed topography is steep. At the steep bathymetry along the shallow part of the north Faroe slope (∼700–1100 m), Semper et al. (2020) have recently discovered the presence of the so-called Iceland-Faroe Slope Jet (IFSJ; **Figure 1**). This jet brings intermediate depth waters from the Iceland Sea toward the southeastern Norwegian Sea. Numerical model outputs suggest the presence of an even stronger deep flow farther north, where the seabed deepens from about 2000 to 3000 m (Dale, 2019). A standard meridional monitoring section (Section N, **Figure 1**) cuts across these two deep flow cores (Hansen and Østerhus, 2000). These observations have hitherto primarily been used to estimate transports of the Atlantic inflow, although recent studies have also focused on

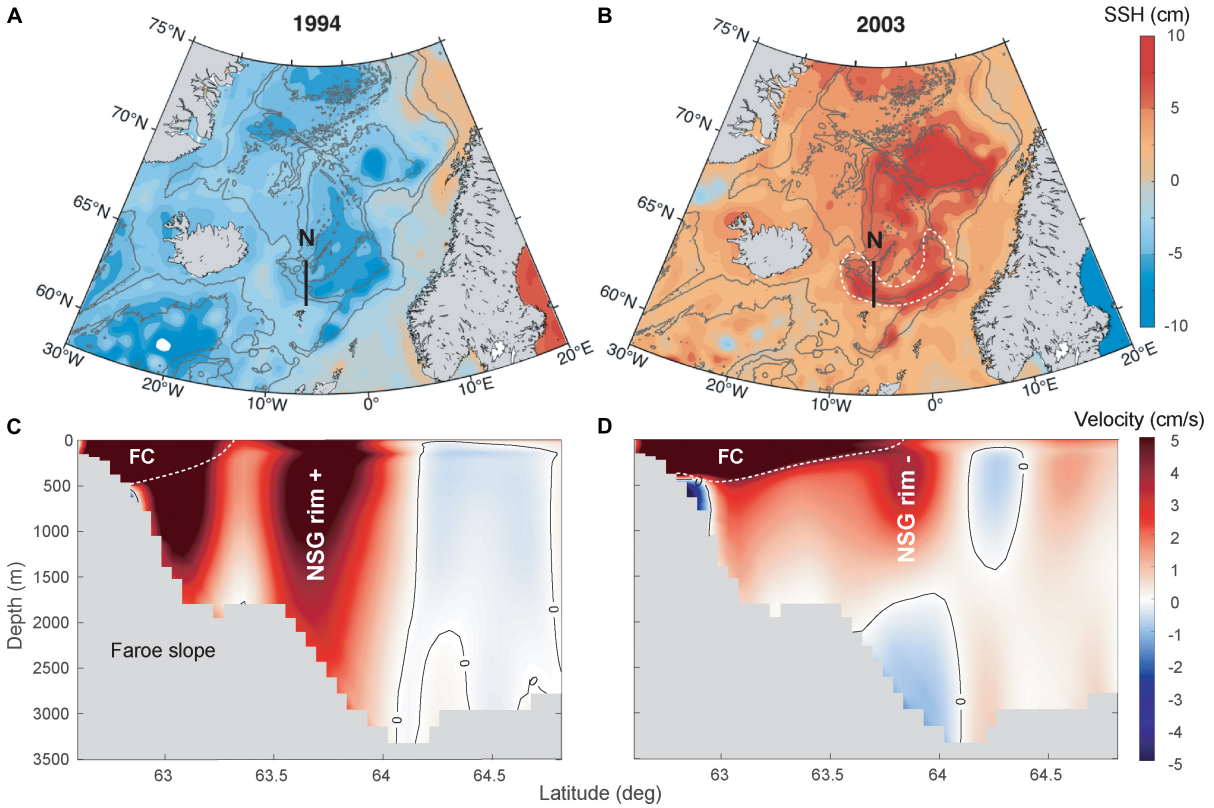

FIGURE 2 | Contrasting states of the NAO and the Norwegian Sea Gyre. Left panels show a NAO+/NSG rim+ state (year 1994) and the right a NAO−/NSG rim− state (year 2003). The upper panels show annually averaged SSH anomalies (deseasonalized and detrended satellite altimetry data) and the lower panels show annually averaged simulated eastward current velocities through Section N (black lines in **A,B**). The approximate position of the interface (dashed white curves in **C,D**) marks the lower boundary of the Faroe Current (FC). The horseshoe-shaped band is illustrated in **(B)** with the dashed white outline.

the influence of the deeper IFSJ (Semper et al., 2020), and the eastward flow of Modified East Icelandic Water (MEIW) (Kristiansen et al., 2016, 2019). Dynamics of the deep flow core (between the 2000 and 3000 m isobaths), which likely carries the highest transport through Section N, has not been studied previously.

Climatic changes are expected to have strong impacts on high latitude oceans, and this calls for continuous and comprehensive monitoring of key aspect of these waters. The recent results by Chafik et al. (2020) and Semper et al. (2020) warrant an updated understanding of the deep flows in the southern Nordic Seas, and modern ocean science aims at a thorough integration of physical, biogeochemical and biological characteristics of such systems. Our motivation with the present study is to start meeting these challenging demands.

By combining hydrographic data from the northern part of Section N, spatio-temporally comprehensive satellite altimetry, updated inventories of Lagrangian Argo data, and model simulations we show that the fundamental aspects of the Norwegian Sea – the NSG, the interface height and the FBCO – are actually interlinked. This provides a new perspective on the Norwegian Sea and its surroundings, which could enable a more holistic understanding of climatic, oceanographic, and ecological aspects of this biologically rich region. Based on this new knowledge, we want to construct key indicator records, which could guide interdisciplinary work in this complex northern region, in a similar way as the SPG index has successfully done for the North Atlantic. The article is organized as follows. Data and methods are presented in section "Data and Methods," results in section "Results" before these are discussed in section "Discussion." The section "Conclusion and Outlook" ends the article.

DATA AND METHODS

Numerical Simulations – NEMO

We use the three-dimensional velocity, temperature, and salinity fields from a simulation of the global ocean using the NEMO ocean model, version 3.6. The simulation, ORCA0083-N001, uses a global grid of nominally 1/12° horizontal resolution and 75 vertical z-star levels. We choose to use a relatively high-resolution model since it is able to explicitly resolve much of the mesoscale eddy–eddy and ocean–atmosphere interactions but also the narrow boundary currents. This is unlike lower resolution models, where such processes are not well represented. The ocean model is forced by the DRAKKAR forcing set v5.2, which is based on the ERA-40 and ERA-interim reanalysis for the

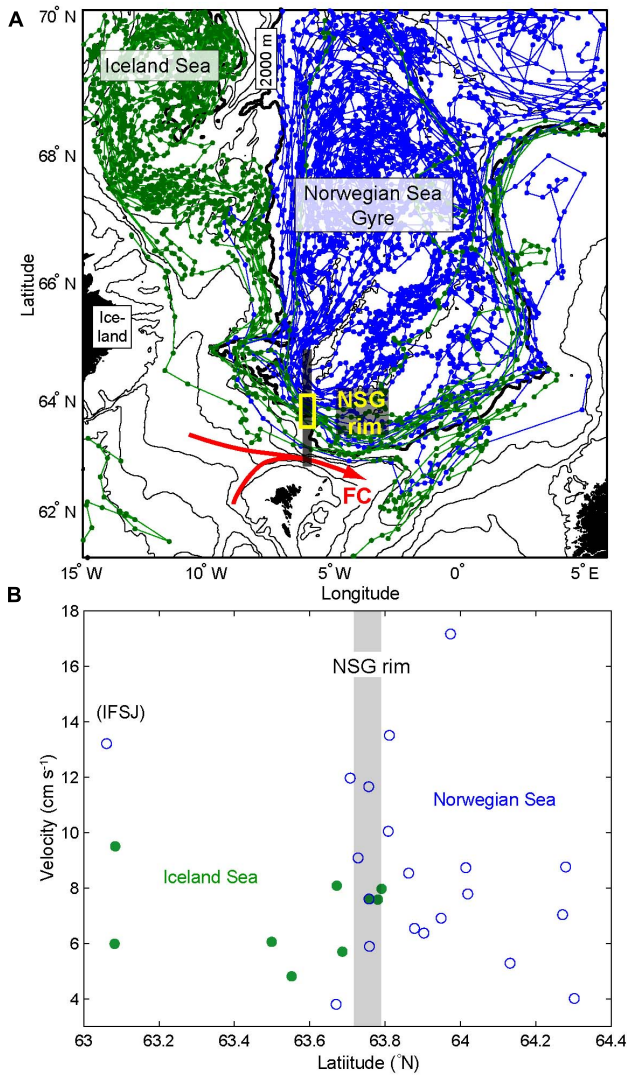

FIGURE 3 | Argo floats. **(A)** Drift trajectories of all available floats which have occupied the Iceland Sea (green) and the Norwegian Sea (blue), respectively. The semi-transparent black line represents Section N, the yellow rectangle shows the location of the NSG rim and the red arrow outlines the Faroe Current (FC). **(B)** Current velocities (*y*-axis) of all the floats crossing Section N, from the Iceland Sea (green) and the Norwegian Sea (blue), respectively. The drift velocities are obtained by interpolating spatially onto this section.

1958–1978 and 1979–2010 period, respectively. The simulation is free-running except for a restoring of sea-surface salinity toward climatology. The model was started from rest in 1958 and run until 2010 (the model output before 1979 is discarded as a model spin-up). In the present work, we only use annual mean zonal velocities along Section N.

Float Trajectories

Float trajectory data are obtained from an Argo-based deep displacement dataset named ANDRO (Ollitrault et al., 2020). The ANDRO atlas ASCII file[1] contains the float parking pressure and temperature, deep and surface displacements, and associated times and deep and surface-associated velocities with their (roughly) estimated errors. From the NetCDF public Argo files, ANDRO first generate a dataset, called DEP (for déplacement, meaning displacement in French) that comprises all the useful information given by the various floats (Ollitrault and Rannou, 2013). Then, the data are checked, corrected, and improved with information gathered outside or through a decoding of the original raw data files. From the final DEP files, the ANDRO atlas is generated. A deep displacement is defined as the distance between the last Argos (or GPS) fix and the first Argos (or GPS) fix of two consecutive cycles.

Hydrographic Data

Section N

Standard Section N consists of 14 stations, labeled N01 to N14, that extend northwards from the Faroe Islands (62.30°N, 6.08°W) into the Norwegian Sea (64.5°N, 6.00°W) (**Figures 1–4**). Since 1988, there have been up to five CTD cruises each year covering this standard section with casts down to the seafloor, or to 1300 m where the bottom depths exceed this value. The maximum bottom depth is 3300 m (at station N14). Typically, cruises have been made in late February, mid-May, late August/early September and early November. After 2011, the monitoring effort was reduced to three cruises each year (the November cruise was terminated).

Large-Scale Data Collection

We use a high-resolution regional (Nordic and Barents Seas) hydrographic database produced by the National Oceanographic Data Center (Korablev et al., 2014) and previously used by e.g., Chafik et al. (2015). It is a compilation of all available data (37 different) sources for the area bounded by 60–82°N, 40°W–70°E (Korablev et al., 2014). This database merges all available oceanographic measurements into one single gridded product. The spatial resolution is 0.25° × 0.25° and annual means have been analyzed. The data have been extensively checked for quality and biases, arising from instruments, were eliminated from the data used in this hydrographic Atlas. Between 1992 and 2012, which is the time period under consideration here, about 60,000 temperature profiles have been compiled in the Nordic Seas. The position of the interface is estimated by the depth of the 3°C isotherm.

Satellite Altimetry

We utilize daily multi-mission satellite altimetry (Pujol et al., 2016) to study the SSH spatial patterns associated with the FBCO transport, the NSG and vertical undulations of the interface. The grid resolution is 0.25° × 0.25° and the period under investigation is between January 1993 and April 2016.

Geostrophic Velocities

Since no direct current observations are available north of the Faroe Current (FC; between stations N08 and N11, described

[1]https://www.seanoe.org/data/00360/47077/#66657

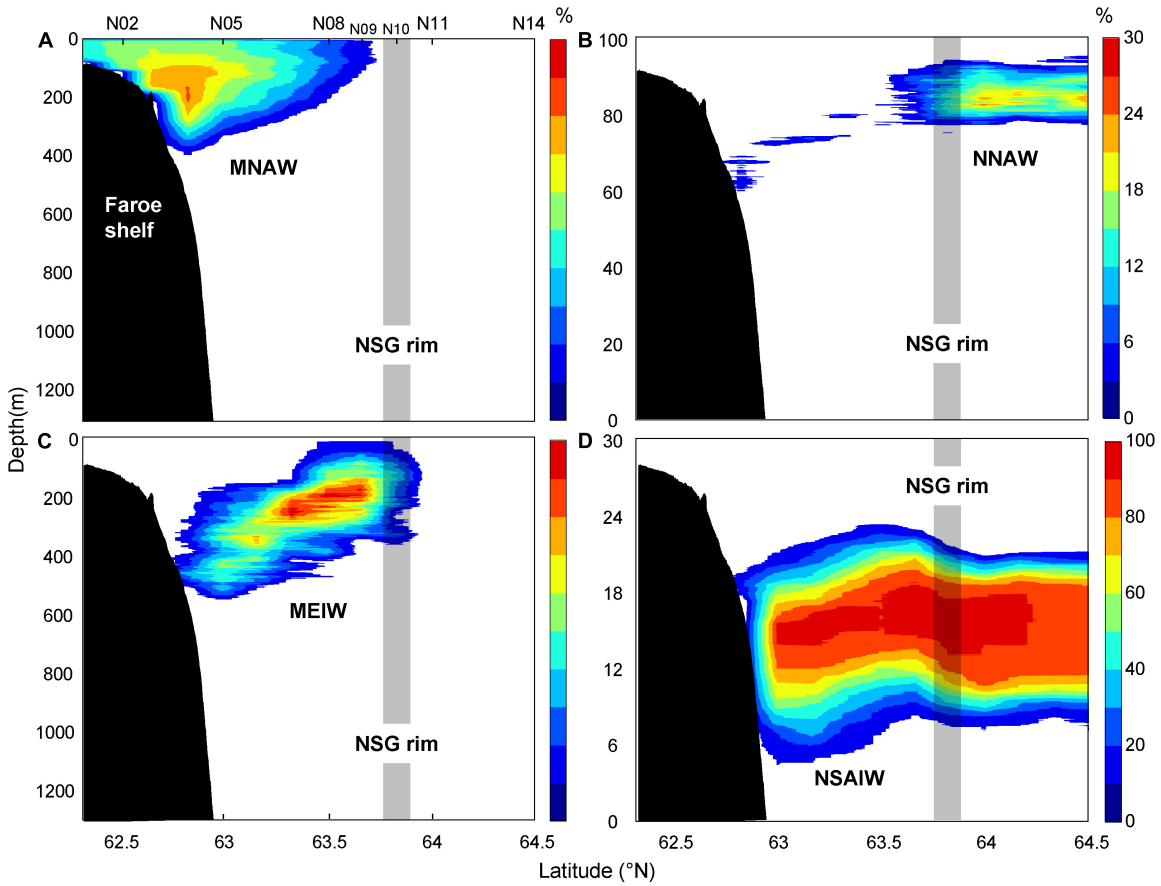

FIGURE 4 | Distribution of the main water masses at Section N (percentages of 103 complete transects between 1988 and 2019 that each latitude-depth data pixel meets the source water mass temperature and salinity criteria in **Table 2**). **(A)** MNAW, **(B)** NNAW, **(C)** MEIW and **(D)** NSAIW. Water mass abbreviations are written in full in **Table 2**. The approximate location of the NSG rim is emphasized with gray bars, and the position of selected standard hydrographic stations are shown in **(A)**.

below), we have to rely on hydrographic data there. By using the thermal wind relation (Cushman-Roisin, 1994), vertical changes in current velocity are proportional to lateral changes in seawater density

$$\frac{\partial u(y,\ z,\ t)}{\partial z} = \frac{g}{\rho_0 f}\frac{\partial \rho(y,\ z,\ t)}{\partial y} \tag{1}$$

where y is lateral (here meridional) distance, z is depth, t is time, g is the gravitational acceleration, ρ_0 is an average density, and f is the Coriolis parameter. Semper et al. (2020) calculated current velocities in the IFSJ region, referenced to the depth of the σ_θ = 27.8 isopycnal ($h_{27.8}$). This isopycnal separates AW from underlying potential overflow water sources. The same approach is used here, but for the deeper current core. Velocity profiles, relative to a reference depth z_0, are in general terms given by

$$u\,(y,\ z,\ t) = \frac{g}{\rho_0 f}\int_{z_0}^{z}\frac{\partial \rho(y,\ z,\ t)}{\partial y}dz \tag{2}$$

here estimated by

$$u_{N,n}\,(y_N,\ z,\ t_n) = \frac{g}{D\,\rho_0 f}\sum_{z_0}^{z}\Delta\rho_{N,n} \tag{3}$$

where N refers to the station numbers (1,…,14), n refers to section number (1,…,103), D = 18.52 km is the distance between the standard stations (10 nautical miles), and $\Delta\rho_{N,n}$ is the density difference between adjacent stations: $\rho\,(y_N,\ z,\ t_n) - \rho\,(y_{N-1},\ z,\ t_n)$. In this study, z_0 is chosen at $h_{27.8}$, and is therefore different for each hydrographic station.

Statistics

Pearson's linear correlation coefficients are calculated using the Matlab® function "corr.m." The presented p-value is the probability of getting a correlation as large as the observed value by random chance, when the true correlation is zero.

RESULTS

Contrasting NAO+ and NAO− States

Annual average conditions during years following particularly NAO high (1994) and NAO low (2003) winters, respectively, are illustrated using altimetry data and simulated current velocities through Section N (**Figure 2**). SSH is depressed/elevated

throughout the NE Atlantic and the Nordic Seas during 1994/2003 (**Figures 2A,B**).

This contrast is particularly pronounced along a horseshoe-shaped band extending from east of Iceland, through Section N and farther eastward along the Norwegian slope. The simulations clearly show two deep flow cores north of the Faroe slope (**Figures 2C,D**). These are resting against steep segments of the Faroe slope roughly between 1000 and 2000 m depths and between 2000 and 3000 m, separated by a region (63.2–63.6°N) with a gentler meridional topographic slope. And the model shows that both cores are much weaker during 2003 (NAO−, **Figure 2D**) as compared to 1994 (NAO+, **Figure 2C**). It should be noted that weakened or even reversal (westward) of the deep flows under the FC core during weak atmospheric forcing such as during 2003 (blue region in **Figure 2D**) have previously been verified by direct current observations (Chafik et al., 2020). No Eulerian current observations are available from the deeper jet. It should also be noted that AW flow in the FC appears to be narrower when the deep jet is strong (1994, dashed curve in **Figure 2C**) and wider when the deep jet relaxes (2003, **Figure 2D**). These results suggest a link between wind forcing, deep flow as well as the main interface between the overlying AW and the underlying denser subarctic waters. And that these processes, furthermore, induce a clear imprint on the SSH field.

Mid-Depth Circulation and Temperatures From Argo Floats

Trajectories of Argo floats show that deep flows from the Iceland Sea (green tracks in **Figure 3A**, all floats parked at 1000 m) and southward deep flows along the Jan Mayen Ridge (floats from 1000, 1200, and 1500 m, blue tracks) merge upstream of Section N. After this confluence, the mid-depth flow concentrates and accelerates along the relatively steep topography north of the Faroe slope (2000–3000 m), whereafter the flow again fans out into 2–3 eastward slower current branches (**Figure 3**). The latitude and speed of the floats, where they cross Section N, is estimated by linear interpolation. Three floats passed under the core of the FC (63.0–63.2°N) – two from the Iceland Sea likely associated with the IFSJ (green dots, **Figure 3B**) – and one from the Norwegian Sea (blue circles). However, the bulk of the floats crossed the section between 63.6 and 64.0°N (**Figure 3B**), with those from the Iceland Sea generally aligning on the southern/shallower side of the jet, and those from the Norwegian Sea congregating on the northern/deeper flank. The 10-days averaged Argo drift velocities in this deeper jet vary between 4 and 17 cm s^{-1} (**Figure 3B**), with an average of 9 cm s^{-1}. Only floats that are parked at 1000 m depths experience drift velocities faster than 10 cm s^{-1}, while those at 1200 and 1500 m did not reach this velocity (depth not shown). The float data thus indicate a mid-depth intensified flow.

We will hereafter refer to the deep jet as the *NSG rim*. Since most floats within the NSG complex are sooner or later being transported by the NSG rim, we postulate that the transport within this narrow and intensified flow represents the circulation strength of the NSG as a whole. We also suggest that this might be an ideal location for monitoring the NSG.

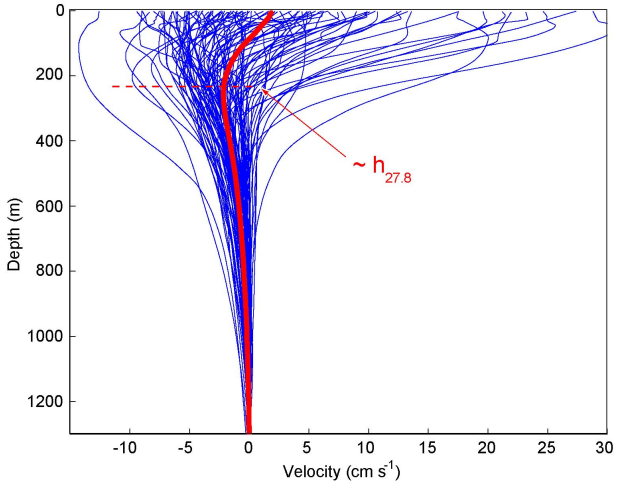

FIGURE 5 | Geostrophic eastward velocity calculations in the NSG rim (between standard stations N09 and N10), relative to z = 1300 m (deepest available data). The blue profiles represent individual occupations of Section N and the averaged of these is shown with the red profile. The average depth of the σ_θ = 27.8 surface ($h_{27.8}$) at this locations, is highlighted.

The NSG Rim at Section N

A Water Mass Boundary

Water mass distributions along Section N (**Figure 4**), are illustrated as percentages (out of 103 complete transects between 1988 and 2019) that each latitude-depth data pixel meets the source water mass temperature and salinity criteria in **Table 2** – adjusted from Hansen and Østerhus (2000). This shows that the NSG rim represents a division zone between the main water masses observed along Section N. It is: (i) the northern limit of the (MN)AW wedge (**Figure 4A**), (ii) the southern limit of the Norwegian North Atlantic Water (NNAW; **Figure 4B**), and (iii) the northern limit of the MEIW tongue (Read and Pollard, 1992; **Figure 4C**). Influence of the NSG rim is also evident at depth by the northward deepening vertical boundaries of the Norwegian Sea Arctic Intermediate Water (NSAIW; 400–800 m, **Figure 4D**). Norwegian Sea Deep Water (NSDW) resides below NSAIW and these two constitute the main overflow source waters (Hansen and Østerhus, 2000).

Limitation Using Satellite Altimetry

Several studies have used satellite altimetry data (SSH) for estimating transports in surface currents (Chafik et al., 2015) – an approach also used for estimating AW transports in the FC (Hátún and McClimans, 2003; Hansen et al., 2015). However, strong near-surface variability (depths > $h_{27.8}$), associated with the variable northward extension of AW (Hansen et al., 2020), prevents us from utilizing altimetry to estimate the deep current variability in the NSG rim. The noise in the upper water above $h_{27.8}$ is much larger than the signal below. It is, however, worth mentioning that the highest correlations between the geostrophic surface current velocities based on the thermal wind relation (referenced to 1300 m) and the SSH gradient from satellite altimetry are indeed identified in

the NSG rim (**Supplementary Figure 2A**). Here, the water column density profile leads the SSH by about a week (**Supplementary Figure 2B**).

A Baroclinic NSG Rim Transport – ψ_{NSG}

Because of the limitation with satellite altimetry, we adopt the approach by Semper et al. (2020), and calculate geostrophic velocities relative the 27.8 kg m^{-3}, and thus to the $h_{27.8}$ depth level. Velocity profiles (relative to 1300 m) in the core of NSG rim (between stations N09 and N10) show that the eastward flows on average weaken up to 200–300 m depths, above which they tend to intensify again (**Figure 5**). This local velocity minimum is generally co-located with $h_{27.8}$. The increase in average velocity from $h_{27.8}$ to 1300 m – a feature unique to the NSG rim (see **Supplementary Figure 1**) – reflects the mid-depth intensification of this deep current jet.

An estimate of the baroclinic NSG rim transport (ψ_{NSG}) is constructed by vertically integrating the geostrophic velocity profiles (see section "Geostrophic Velocities") from $h_{27.8}$ and downwards. From each individual transect (n), we select the highest obtained value within the meridional window between hydrographic stations N08 to N11 (see **Figure 4A**), in order to account for lateral shifts of the NSG rim. This is given as:

$$\psi_{\mathrm{NSG}}(t_n) = W \cdot \max_{N\in\{N08,\ldots,N11\}} \left[\int_{h_{27.8}}^{D} u_{N,n} dz \right] \quad (4)$$

Where $u_{N,n}$ is given by eq. 3 down to 1300 m depth, and where we extrapolate the estimated baroclinic velocity at 1300 m down to the seafloor (see also **Figure 5**). This might be a slight overestimation, since the NSG rim seems to be mid-depth intensified. D and W are unknown representative depths and widths of the NSG rim. The latitudinal position of the NSG rim core shifts between stations N08–N09 (11%), N09–N10 (49%), and N10–N11 (40%). Although the averaged signature of the NSG rim might therefore influence a $\sim$ 60 km wide swath, synoptic CTD sections reveal a narrower jet, often localized between two hydrographic stations (18.52 km apart). We thus estimate the representative width to 20–30 km. A representative depth, from $h_{27.8}$ to an average bottom depth at these stations, must lie in the range 2–2.5 km.

Statistics of an upper and a lower estimate of ψ_{NSG}, respectively, are provided in **Table 3**. The median value is in the range 1.5–2.4 Sv (relative to $h_{27.8}$), and there is a seasonal variation with the strongest relative transport during February (1.9–3.5 Sv) and the weakest transport during late summer cruises, August/early September, (−0.8 to −1.6 Sv, westward transport relative to $h_{27.8}$). The transport was high around 1999–2000, but 2–3 years after (2002–2003) the low-passed ψ_{NSG} had weakened by about 4–7 Sv (**Table 3** and see **Figure 7**) – given no velocity changes at the $h_{27.8}$ depth level. Differences between individual extreme transects, however, exceed ten Sverdrups (not shown).

The wind stress curl driven barotropic component of the NSG circulation is strong (e.g., Nøst and Isachsen, 2003), and the current velocities at $h_{27.8}$ are therefore not zero. This obvious limitation in the baroclinic ψ_{NSG} can probably not be overcome with the presently available observational material. The barotropic flow is, however, in phase with ψ_{NSG}, with maximum cyclonic circulation during winter and NAO+ years (e.g., 1999–2000), and much weaker circulation during summer and NAO− years (e.g., 2002–2003) (Jakobsen, 2003). ψ_{NSG} should not be regarded as an absolute measure, but rather a conservative (underestimated) metric of the NSG circulation intensity.

Contrast Between Strong and Weak ψ_{NSG}

A composite analysis is made by contrasting averages of sections with the ten highest values of ψ_{NSG} (out of 103) (NSG+ state) against averages of the ten lowest ψ_{NSG} values (NSG− state). This reveals the following: A strong NSG rim (**Figures 6A,B**) entails a generally uplifted $h_{27.8}$ and thus a narrow AW wedge, increased volume of MEIW (visible as a low salinity wedge between AW above and NSAIW below, **Figure 6B**), and a fresh top (0–100 m) funneled over the NSG rim (63.5–64.0°N). A weak NSG, on the other hand (**Figures 6C,D**), relates to an additional AW core in the 63–63.6°N latitudinal band (particularly visible in the salinity field, **Figure 6D**), and a northward shift of the surface front to around 63.8°N. The fresh top layer is laterally spread out north of the front during this state.

ψ_{NSG} is significantly correlated to the interface height averaged over the region with a variable northern AW core (63–63.6°N), both when comparing individual transects and after applying the five-transect low pass filter (R $\sim$ −0.7). In this region, the interface is about 150 m higher during NSG+ states, compared to NSG− states (cf. **Figures 6A,C**). This contraction/spreading of the AW wedge is in general agreement with the simulations (**Figures 2C,D**).

As illustrated with the contrasting years 1994 vs. 2003, this interface undulation also influences the SSH (**Figures 2A,B**). On a more local scale strong station-by-station correlations are found between the steric height (relative to 800 m) in this region, and the SSH at the nearest satellite altimetry grid-point (**Table 4**).

A Broader View

Links Between ψ_{NSG}, FBCO, and SSH

The NSG rim baroclinic transport ψ_{NSG} is linked to both the FBCO (**Figure 7B**, R = 0.85, $p < 10^{-18}$, N = 86) and SSH north of the IFR (**Figure 7A**, R = 0.74, $p < 10^{-11}$,

TABLE 3 | Statistics of the NSG rim transport (ψ_{NSG}), provided as a lower estimate (width W = 30 km and average depth D = 2 km, see eq. 4) and as an upper estimate (W = 30 km and average depth D = 2.5 km).

ψ_{NSG}	Median	Standard error (SE)	February	September	NSG+ (1999–2000)	NSG− (2002–2003)
Lower	1.3 Sv	0.3 Sv	1.9 Sv	−0.8 Sv	3.2 Sv	−0.7 Sv
Upper	2.5 Sv	0.6 Sv	3.5 Sv	−1.6 Sv	6.0 Sv	−1.4 Sv

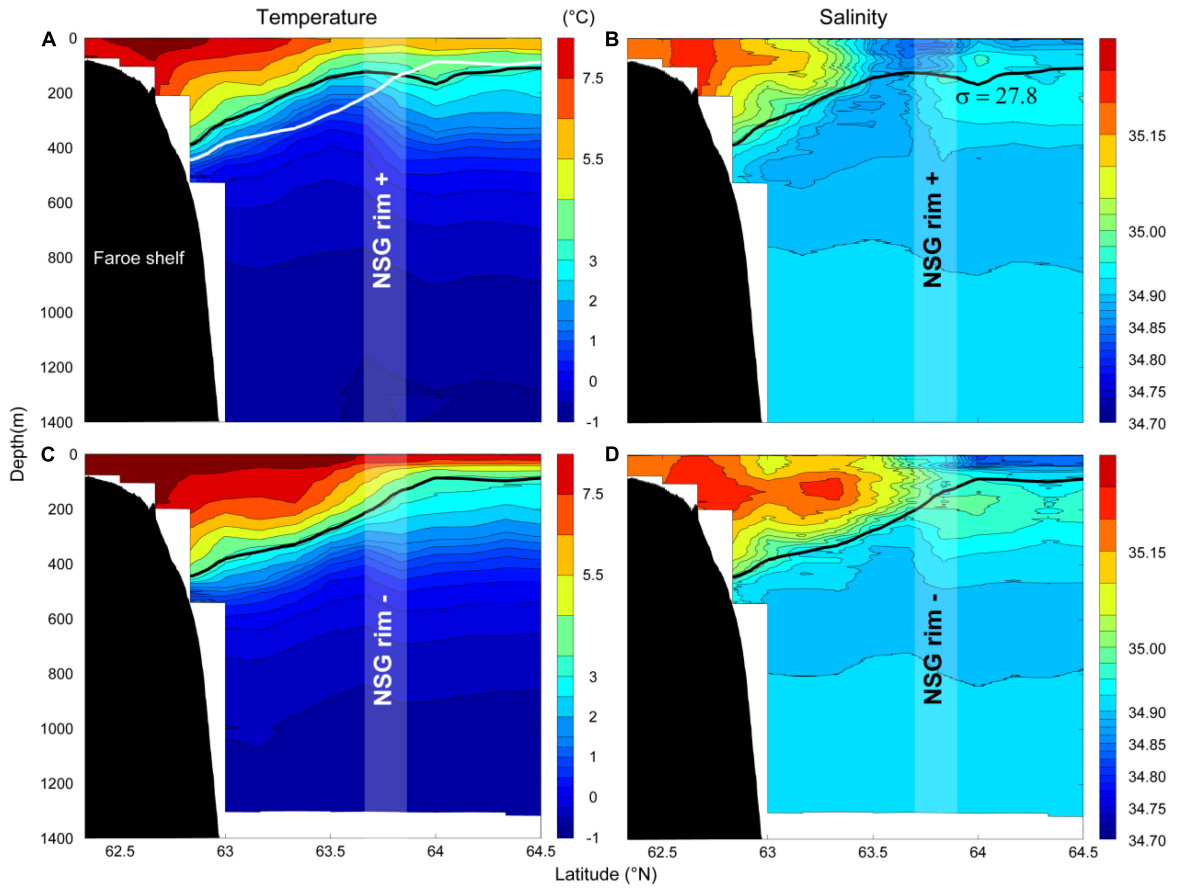

FIGURE 6 | Hydrographic composite sections, contrasting periods with a strong NSG rim **(A,B)** against periods with a weak NSG rim **(C,D)**. The states are represented by an average over ten sections with the highest and lowest value of ψ_{NSG}, respectively. Black lines show the position of the σ_θ = 27.8 isopycnal ($h_{27.8}$) during NSG rim+ and NSG rim– states, respectively. The white line in **(A)** shows $h_{27.8}$ from **(C)**.

N = 86), where the interface height is tightly linked to the FBCO (Köhl, 2010) and where strong SSH variability is observed (**Figures 2A,B**). This region is hereafter referred to as *IFR-North*. In order to smooth out the seasonal signal, the FBCO and the SSH series were low-pass filtered using a running mean (over 360 days), while ψ_{NSG} was low-passed using a Butterworth filter (width of four data points, corresponding to one year). The monitoring of Section N was reduced in 2011 from 4–5 annual transects to three transects, which has made the extraction of a reliable inter-annual signal less reliable (Hátún et al., 2005b). The years after 2011 have therefore been omitted from this correlation analysis and from **Figure 7**.

The extreme shift from a strong NSG rim in 1999–2000 to a weak NSG rim in 2002–2003 (**Table 3** and **Figure 7**) concurred with both a shift from weak FBCO to the highest FBCO transport on record (**Figure 7B**), and a marked increase in SSH in the IFR-North region (**Figure 7A**). Having established a link between ψ_{NSG} and the FBCO, we use the latter record (which is represented by daily sampling) to explore linkages between the NSG/FBCO system and the interface/SSH fields.

Links Between FBCO and the Interface

The FBCO is negatively correlated to the interface height along the horseshoe shaped band mentioned in section "Contrasting NAO+ and NAO− states" (**Figures 2**, **8A**). Particularly strong and statistically significant correlations (blue color) are evident in the IFR-North region and along the edge of the Vøring Plateau. That is, strong/weak overflow relates to depressed/shoaled interface in these regions. The interface position was represented as the depth of the 3°C isotherm, obtained from the gridded hydrographic data set (see section "Large-Scale Data Collection").

In contrast, the FBCO variability is positively correlated with the interface height along a narrow band following the Norwegian and Shetland slopes (red colors in **Figure 8A**), which generally overlays the deep FSCJ (**Figure 1**; Chafik et al., 2020). Thus strong overflow concurs with a higher interface over the FSCJ – and thus a banking up of cold and dense water along the continental slope.

Links Between FBCO and SSH

Correlation analysis between the daily records of FBCO transport and the gridded altimetry data reveals a close link between the

TABLE 4 | Correlation analysis between the steric height (relative to 800 m) and SSH.

Station	*N*	Standard	R_0	a_0	Significant
N05	87	6.74	0.77	0.85	$p < 0.001$
N06	79	7.48	0.77	0.78	$p < 0.001$
N07	82	7.72	0.84	0.78	$p < 0.001$
N08	80	7.47	0.83	0.68	$p < 0.001$
N09	79	7.10	0.80	0.48	$p < 0.001$
N10	79	6.69	0.67	0.33	$p < 0.001$

*Data from six standard hydrographic stations along the central part of Section N (see **Figure 4A**) and the nearest satellite altimetry grid-points are used. N is number of data points and R_0 and a_0 are the correlation and the regression coefficients, respectively.*

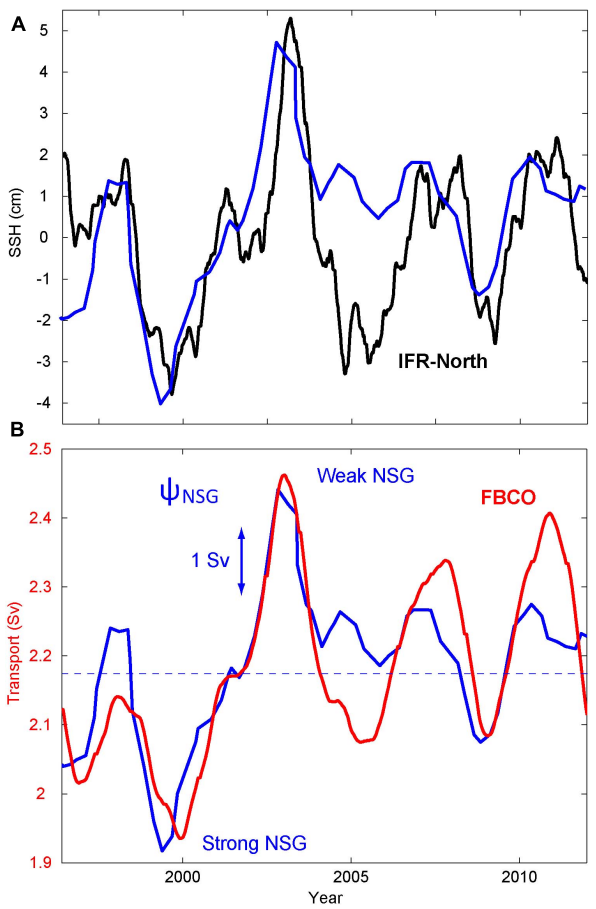

FIGURE 7 | Time series of the baroclinic NSG rim transport ψ_{NSG} (blue), compared to **(A)** sea-surface height north of the Iceland-Faroe ridge (IFR-North, black), and **(B)** the FBCO transport (red). ψ_{NSG} is here estimated using representative depth and width of D = 2 km and W = 30 km, respectively (**Table 3**). ψ_{NSG} is not an absolute measure of transport (therefore no values are provided on the y-axis), and the magnitude of inter-annual changes is illustrated by the blue double arrow in **(B)**.

FBCO transport and SSH in the IFR-North region, even on weekly time scales (**Figures 8B**, **9**, $R > 0.8$). The series are high-pass filtered by subtracting the 360-days running mean, in order to remove the pronounced annual cycle. Our observations thus support those previous model results. High FBCO vs. SSH correlations also appear east of the Vøring Plateau – where strong negative FBCO vs. interface correlations were found (**Figure 8B**).

This close coupling between FBCO and both interface heights and SSH in the IFR-North region points to the action of a common and direct driver. In the discussion, we propose the NSG circulation, and ultimately the action of the wind stress curl (Nøst and Isachsen, 2003), as this driver.

DISCUSSION

The NSG Rim

The here presented Argo floats trajectories show that intermediate source waters from the Iceland Sea and the southward flow along the Jan Mayen Ridge converge north of the Faroe slope, where the seafloor steeply deepens from 2000 to 3000 m depths (**Figures 2**, **3**). This region is here referred to as the NSG rim.

A meridional monitoring section, Section N, crosses both the Atlantic inflow in the FC and the NSG rim (**Figures 1**, **4A**), and we provide the first utilization of data from the deeper parts, i.e., away from the slope, of this valuable monitoring section. Direct current observations are not available from the NSG rim (hydrographic standard stations N09–N10, see **Figure 4A**), but Argo trajectory data reveal relatively strong mid-depth (1000–1500 m) currents in the NSG rim. Furthermore, there is a congregation of surface drifters[2] in the NSG rim, and their eastward drift velocity is appreciable (not shown).

We show that the NSG rim is a transition zone between the main upper ocean water masses north of the Faroe slope. It forms the northern boundary of the AW wedge, the northern extent of the subducted MEIW tongue, and the southern limit of NNAW (**Figure 4**). Acknowledging the deep-reaching flow in the NSG rim is therefore a prerequisite for understanding the physical oceanography in this important region.

Transport Variability in the NSG Rim

Lacking direct current observations in the NSG rim, we have relied on geostrophic calculations. Thermal wind shear shows that current velocities in the NSG rim generally increases with depth in the more quiescent waters below $h_{27.8}$ (**Figure 5**). Increasing velocities with depth can also occur in the IFSJ (bottom depths 700–1100 m) (Semper et al., 2020), while at all other locations, current velocities decrease with depth (**Supplementary Figure 1**) – which is the more typical condition in the ocean. As a proxy for the intensity of the NSG rim current (ψ_{NSG}), we calculate the eastward transport below $h_{27.8}$ and 1300 m (deepest hydrographic data). Although ψ_{NSG} is temporally coarse (based on only 4–5 data points each year), we can substantiate a close inverse correlation between this proxy record and the temporally well resolved FBCO record. ψ_{NSG} is strong when the overflow is weak and vice versa. Particularly evident is the major change from weak overflow around 1999–2000 (∼1.95 Sv) to the strongest overflow on

[2]http://www.aoml.noaa.gov/envids/gld/dirkrig/parttrk_spatial_temporal.php

record during 2002–2003 (∼2.45 Sv). This event was associated with a decreasing ψ_{NSG} by more than 6 Sv – relative to $h_{27.8}$ (**Table 3** and **Figure 7**). The general near-surface circulation in the NSG likely also decreased from the around 2000 (NAO+) to the latter period, which was characterized by a low NAO (Jakobsen, 2003). The barotropic contribution therefore adds to the presented baroclinic proxy record, and together this is clear evidence of a weakening NSG circulation between these extreme periods. Based on this, we propose the following hypothesis: *The FBCO variability is linked inversely to the strength of the NSG circulation.*

Contrasting NSG+/NSG− States and Possible Drivers

According to Yang and Pratt (2013), our hypothesized link between the NSG circulation and the FBCO must involve sill-level pressures in near-slope regions (at near sill-level depths), and not within the central parts of the Norwegian Sea.

A summary of key elements during contrasting NSG+ and NSG− states is provided in the schematic in **Figure 10**. A NSG− state, and high FBCO transport, are associated with generally elevated SSH in the Nordic Seas, especially along the horseshoe-shaped swath along the boundary current system (**Figures 2A,B**, **8**, **10**). NSG– and strong overflow also links to a depressed interface in this region (red **Figures 8A**, **10**). This latter fact appears to contradict the generally accepted view, that an uplifted interface is required to establish a Norwegian Sea-to-North Atlantic sill-level pressure gradient – and thus strong overflow. The depressed interface reduces the pressure increase from the elevated SSH, but it remains uncertain whether this 'baroclinic compensation' is complete at sill-level-depths (Olsen et al., 2008).

We have, on the other hand, identified a narrower band along the Norwegian and Shetland slopes with positive correlations between the FBCO transport and the interface heights (**Figures 8A**, **10**). Along this band, strong overflow transports (NSG−) are linked to both an uplifted interface and higher SSH, which thus both contribute to increased sill-level pressure. This suggests that collaborative influence of SSH and interface height on the near-bottom pressure along the European continental slope could drive the FBCO transport variability (at least on relatively short barotropic time scales). In this way, cyclonic/anti-cyclonic wind circulation anomalies could directly/regionally impact the poleward AW boundary current and the interface depth along the European continental shelf, which, in turn, regulates sill-level pressures in the FSCJ and the variability in the FBCO (Sandø et al., 2012; Bringedal et al., 2018). That implies that the FBCO is driven by shifting wind regimes, which concurrently drives both the AW boundary current, and the NSG circulation.

However, a release of dense overflow water from the gyre to the adjacent slopes is required to continuously feed the FSCJ and subsequently the FBCO. And these NSG-to-slope exchange processes are likely linked to both the wind stress curl field and the NSG circulation (Yang and Pratt, 2013). A complete description of this system is beyond the scope of the present work, and just a few tentative statements will be provided here. The fact that strong FBCO is associated with weaker eastward flow north of the Faroe slope, both in the shallower IFSJ region (Chafik et al., 2020), and further north in the deeper NSG rim (**Figures 7A**, **9**) remains a conundrum, which warrants further study.

Variable FBCO can exert an upstream feedback effect on both the interface height and SSH over a dense water reservoir just off the Norwegian slope (part of the horseshoe-shaped region between the Faroes and Norway). Anomalies in the FBCO transport can reach 0.5 Sv for extended periods (**Figure 9**), and such a drainage anomaly flux would cause the interface

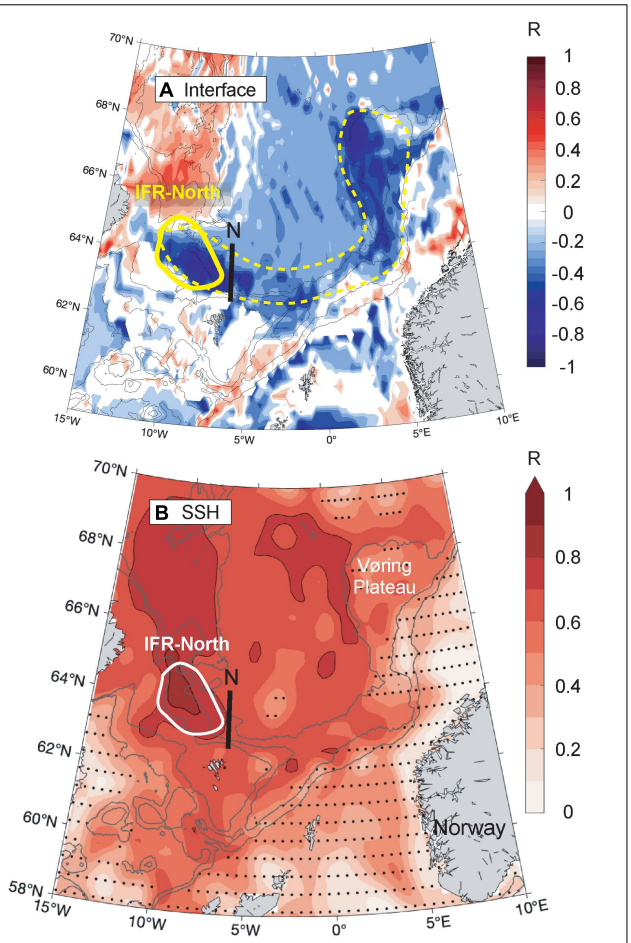

FIGURE 8 | A broader view. Correlation maps between the FBCO transport and **(A)** the height of the 3°C isotherm (see section "Large-Scale Data Collection") and **(B)** the sea-surface height field (SSH) from satellite altimetry. The correlation of the interface in the upper panel is based on annual mean data, while a 360-day running mean is used for the SSHs in the lower panel. Because of the time smoothing, the dotted regions in the lower panel indicate non-significant correlations based on the number of effective degrees of freedom (Pyper and Peterman, 1998). The position of standard hydrographic section N is shown with black lines, and the yellow/white outline in **(A,B)** marks the IFR-North region, from where the SSH time series in **Figure 9** is extracted. The horseshoe-shaped band is illustrated with the dashed yellow outline in **(A)**.

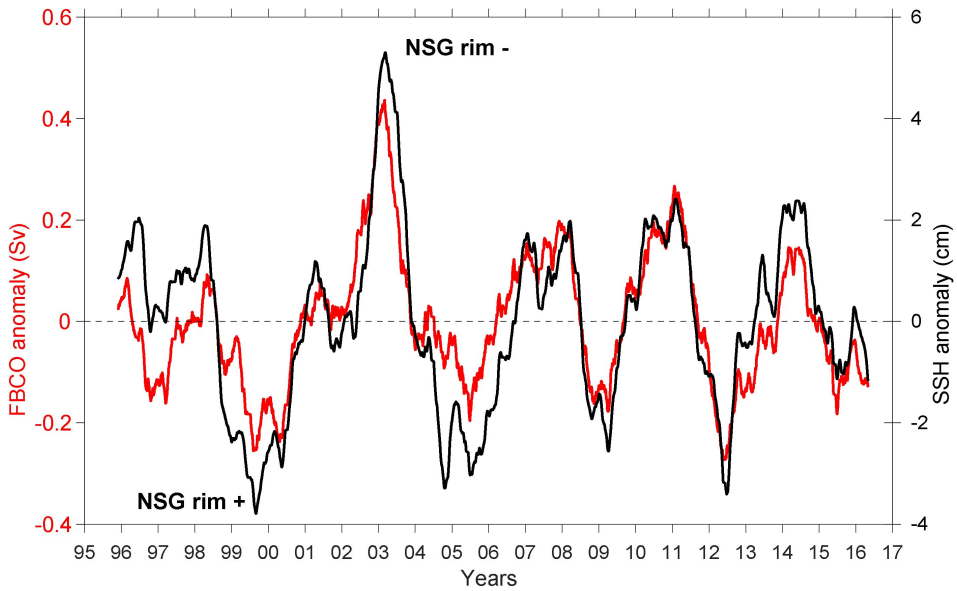

FIGURE 9 | Time series of the FBCO (red) and the sea-surface height (SSH) in the IFR-North region (yellow/white outline in **Figure 8**). The series have been detrended and running mean filtered over 360 days, in order to remove the seasonal signal.

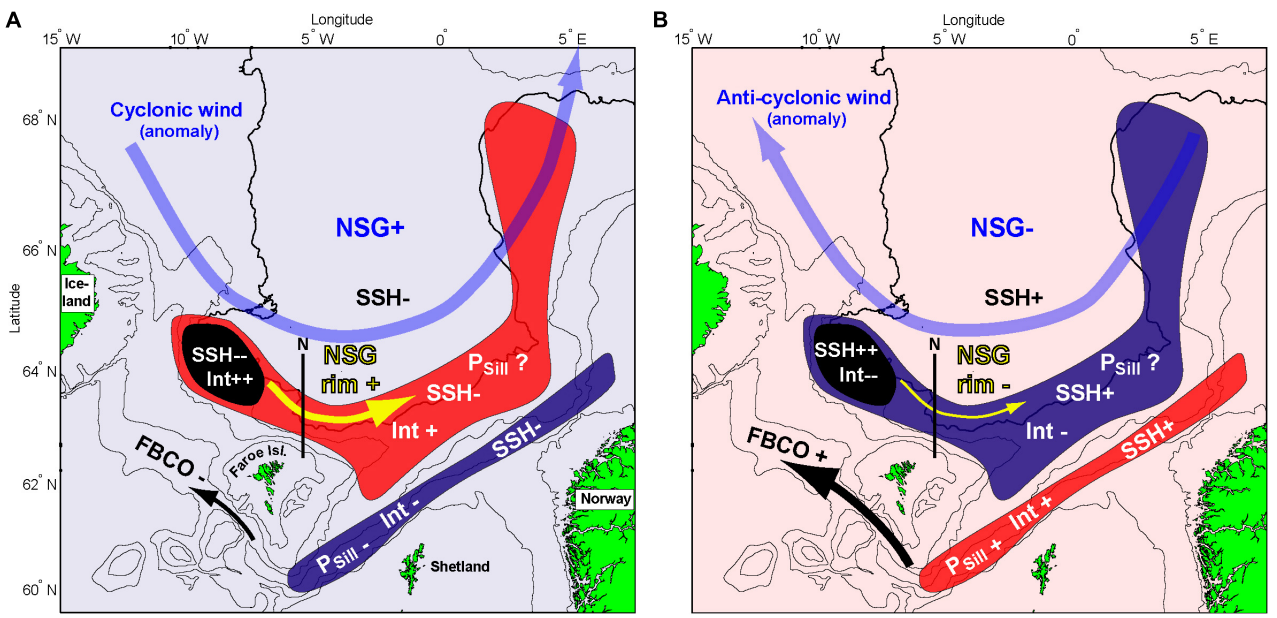

FIGURE 10 | A schematic of key element under contrasting **(A)** NSG+ and **(B)** NSG– states. "Int" refers to the interface height and P_{Sill} refers to the pressure at depth levels of the Faroe Bank Channel sill (~850 m). The other abbreviations are provided in **Table 1**. A "+" refers to a strong value, cyclonic anomaly or elevated level of both the interface and SSH, and opposite for a "–." The weak background colors refer to the broad SSH contrasts, while the more strongly colored regions show the additional imprint of vertical interface movement.

over a realistic source region (~1000 km long and ~100 km wide) to move vertically – about 1 m per day. Persistent FBCO+ periods could therefore notably lower the interface and elevate SSH over parts of the horse-shoe shaped region (blue in **Figure 10B**), while FBCO– states have the opposite effect (red in **Figure 10A**).

The fact that the highest FBCO vs. SSH correlations are identified in the IFR-North region (**Figure 8B**) – and not near the plausible source pathway along the European Continental slope – is likely related to the variable deep currents under the FC, through the mechanisms discussed in Orvik (2004). Weak eastward flows, and even reversals to westward deep flows

(Chafik et al., 2020) during NSG−/FBCO+ states (**Figure 2**) oppose the Atlantic inflow through the Iceland-Faroe gap, causing convergence of AW, deepening of the interface and elevation of the sea surface in the IFR-North region (**Figure 10**). We conclude that SSH changes over the IFR-North do not drive the FBCO changes, but are merely a result of the variable NSG circulation. We suggest that this mechanism can explain the puzzling negative sensitivity between the IFR-North interface height and the FBCO variability, as reported by Köhl (2010).

Other Implications of the Sensitive IFR-North Region

The vertical interface motion in the IFR-North region is in itself of profound oceanographic importance, since it likely relates to Atlantic inflow through the Iceland-Faroe gap (Blindheim, 1990), substantiated by negative correlations between the FC AW inflow and the IFR-North SSH (Hansen et al., 2010). These dynamical linkages might also impact both the IFR overflows as well as water mass contribution from the Iceland Sea (e.g., *via* the IFSJ; Semper et al., 2020) – although these last mechanisms have not yet been demonstrated with observations.

The very close correlation between these two remotely located, and important in its own right, processes (FBCO and IFR-North SSH; **Figure 9**), holds promise for a firmer understanding of the oceanographic variability within and around the Norwegian Sea. Furthermore, the freely available altimetry data can be used to complement the observational record of the FBCO, e.g., in case of instrument failure. The satellite data can, however, not replace the *in situ* current data since the directly observed FBCO contains high frequency variability (less than a week) and long-term trends, which are not captured by the satellites.

Ecological Implications

Contrasting periods with a strong NSG rim (e.g., 1999–2000) against periods with a weak gyre (e.g., 2002–2003) reveals fundamental oceanographic changes in the southern Norwegian Sea, which likely reverberate in ecosystems.

A strong NSG draws large amounts of MEIW and likely also of Arctic intermediate water masses from the Iceland Sea (**Figure 6B**), and these contain high concentrations of large and lipid-rich zooplankton types (*Calanus hyperboreus* and large overwintering stages of *Calanus finmarchicus*) (Kristiansen et al., 2016, 2019). The marked NSG weakening after 2002 resulted in a wider (northward extended) AW wedge, and a deeper interface at the northern flank of the FC. This increased AW influence entailed phenological changes as, e.g., the numbers of the younger stages in the *C. finmarchicus* population markedly increased, while the abundance of both overwintering *C. finmarchicus* and *C. hyperboreus*, sampled in May, decreased (Kristiansen et al., 2016).

Furthermore, large mesopelagic biomass congregates along the AW/subarctic water interface, which by acoustic monitoring is identified as the so-called Deep Scattering Layer (Hays, 2003). A depressed interface extends the range of the Daily Vertical Migration of mesopelagic biomass – from the interface during day to the near-surface feeding zone during night (Cisewski et al., 2021).

Herring (*Clupea harengus*) selectively prey on the mentioned relatively large zooplankton species (Dalpadado et al., 2000). This fish species does also perform Diel vertical migrations and during the May feeding season, it congregates in the confluence region between Iceland Sea and Norwegian Sea water masses, which exhibits contrasting changes in the 3°C isotherm depth (65–66°N, 6–8°W; **Figures 3**, **8A**). This is just north of the highest FBCO vs. SSH correlations, which underscores the likely ecological significance of the records presented here.

CONCLUSION AND OUTLOOK

While inflowing warm AW into the Nordic Seas toward the Arctic and returning dense overflow water at depth are typically studied separately, we here show that the variability in these key flows is intrinsically coupled. The connections involve both vertical undulations of the main interface – which separates the warm and cold waters – and the circulation strength of the NSG. We provide the first record of baroclinic transport variability in this gyre, based on hydrographic data from a standard section (Section N), which crosses the strongest and most focused flow of the NSG. This NSG rim is guided by the steep bathymetry between 2000 and 3000 m bottom depths and its presences divides the main water masses in the southwestern Norwegian Sea. During periods with strong NSG (and weak FBCO), the wedge of AW is narrow, and the interface around the southern and eastern rim of the Norwegian Sea is generally elevated – and vice versa for weak NSG/strong FBCO. These linkages are, however, opposite in shallower waters close to the Norwegian and Shetland slopes, where strong NSG/weak FBCO is associated with a depressed interface. The sea level topography in the biologically rich confluence region north of the IFR is highly sensitive to variability in the NSG/FBCO system. The low temporal resolution of standard hydrographic sections is at the detection limit of the herein discussed dynamics. In order to improve the spatial resolution of the NSG region, the Faroe Marine Research Institute (FAMRI) has already added an extra hydrographic standard station between standard station N09 and N10. We furthermore recommend that hydrographic Section N should be occupied at least four times a year, distributed evenly over the seasons. And presently, FAMRI has deployed an upward looking Acoustic Doppler Current Profiler (ADCP) in the NSG rim, in an attempt to increase the vertical and temporal sampling resolution, as well as capturing the barotropic component of this flow. And as demonstrated, high spatio-temporal resolution data provided by satellite altimetry can complement the monitoring of the FBCO transport and, by inference, the NSG strength. The demonstrated connectedness provides a basis for improved understanding of

physical, climatic, and ecological aspects of this dynamic and biologically productive system.

DATA AVAILABILITY STATEMENT

The original contributions presented in the study are included in the article/**Supplementary Material**, further inquiries can be directed to the corresponding author/s.

AUTHOR CONTRIBUTIONS

HH developed the main ideas and did most of the analysis and the writing, in correspondence with LC. LC provided analysis of altimetry data, numerical model output, and hydrographic database. KMHL provided *in situ* data (hydrography and current observations) and supported with the writing. All authors contributed to the article and approved the submitted version.

FUNDING

This study was supported by the European Union's Horizon 2020 Research and Innovation Program under grant agreement no. 727852 (Blue-Action). Data collection along Section N received support from the European Framework Programs under grant agreement numbers GA212643 (THOR), and 308299 (NACLIM) and from the Danish Ministry of Climate, Energy and Utilities through its climate support program to the Arctic (FARMON and FARMON2). LC acknowledges support from the Swedish National Space Agency through the FiNNESS project (Dnr: 133/17).

SUPPLEMENTARY MATERIAL

The Supplementary Material for this article can be found online at: https://www.frontiersin.org/articles/10.3389/fmars.2021.694614/full#supplementary-material

Supplementary Figure 1 | Averaged (over 103 complete transects) geostrophic current velocities, relative to 1300 m depths. Dark red color shows that velocities increase up through the water column, while the other colors demonstrate that velocities decrease up through the water column in the NSG rim. (The tick marks on the *x*-axis are the same as in **Figure 4**).

Supplementary Figure 2 | (a) Correlation coefficients between surface geostrophic currents based on hydrography (relative to 1300 m), SSH gradient (altimetry), respectively. Both are calculated between the standard hydrographic stations, and a daily satellite altimetry product is used. **(b)** Time lags between hydrography and altimetry, where the highest correlation coefficient is obtained (positive values show that hydrography leads). In the NSG rim, the water column density profile leads the SSH by about a week **(b)**. We interpret this curious fact as follows: the vorticity input from winds is efficiently transmitted to the bottom, where the local slope of the *f*/*H* field, through bottom Ekman dynamics, set up near-bottom currents (Nøst and Isachsen, 2003) which subsequently translate up through the NSG after an inertial time lag – which appears to be about a week.

REFERENCES

Blindheim, J. (1990). Arctic intermediate water in the Norwegian Sea. *Deep Res. A Oceanogr. Res. Pap.* 37, 1475–1489. doi: 10.1016/0198-0149(90)90138-l

Blindheim, J., Borovkov, V., Hansen, B., Malmberg, S. A., Turrell, W. R., and Østerhus, S. (2000). Upper layer cooling and freshening in the Norwegian Sea in relation to atmosphere forcing. *Deep Res.* 47, 655–680. doi: 10.1016/s0967-0637(99)00070-9

Bringedal, C., Eldevik, T., Skagseth, Ø, Spall, M. A., and Østerhus, S. (2018). Structure and forcing of observed exchanges across the greenland–scotland ridge. *J. Clim.* 31, 9881–9901. doi: 10.1175/JCLI-D-17-0889.1

Chafik, L., Hátún, H., Kjellsson, J., Larsen, K. M. H., Rossby, T., and Berx, B. (2020). Discovery of an unrecognized pathway carrying overflow waters toward the Faroe Bank Channel. *Nat. Commun.* 11:3721. doi: 10.1038/s41467-020-17426-8

Chafik, L., Nilsson, J., Skagseth, Ø, and Lundberg, P. (2015). On the flow of Atlantic water and temperature anomalies in the Nordic Seas toward the Arctic Ocean. *J. Geophys. Res.* 120, 7897–7918.

Cisewski, B., Hátún, H., Kristiansen, I., Hansen, B., Larsen, K. M. H., Eliasen, S. K., et al. (2021). Vertical migration of pelagic and mesopelagic scatterers from ADCP backscatter data in the Southern Norwegian Sea. *Front. Mar. Sci.* 7:542386. doi: 10.3389/fmars.2020.542386

Cushman-Roisin, B. (1994). *Introduction to Geophysical Fluid Dynamics*. New Jersey: Prentice-Hall, Inc, 1–320.

Dale, A. (2019). *Variabilité Saisonnière de L'écoulement D'eau Dense Dans le Passage du Banc des Féroé*. Thesis. Paris: Laboratoire d'Océanographie et du Climat (LOCEAN), 1–27.

Dalpadado, P., Ellertsen, B., Melle, W., and Dommasnes, A. (2000). Food and feeding conditions of Norwegian spring-spawning herring (*Clupea harengus*) through its feeding migrations. *ICES J. Mar. Sci.* 57, 843–857. doi: 10.1006/jmsc.2000.0573

Hansen, B., Hátún, H., Kristiansen, R., Olsen, S. M., and Østerhus, S. (2010). Stability and forcing of the Iceland-Faroe inflow of water, heat, and salt to the Arctic. *Ocean Sci.* 6, 1013–1026. doi: 10.5194/os-6-1013-2010

Hansen, B., Larsen, K. M. H., and Hátún, H. (2020). *Atlantic water extent on the Faroe Current monitoring section. Havstovan NR.: 20-03 Technical Report*. Faroe Islands: Tórshavn, 1–103.

Hansen, B., Larsen, K. M. H., Hátún, H., Kristiansen, R., Mortensen, E., and Østerhus, S. (2015). Transport of volume, heat, and salt towards the Arctic in the Faroe Current 1993-2013. *Ocean Sci.* 11, 743–757. doi: 10.5194/os-11-743-2015

Hansen, B., Larsen, K. M. H., Hátún, H., and Østerhus, S. (2016). A stable Faroe Bank Channel overflow 1995-2015. *Ocean Sci.* 12, 1205–1220. doi: 10.5194/os-12-1205-2016

Hansen, B., and Østerhus, S. (2000). North Atlantic–Nordic Seas exchanges. *Prog. Oceanogr.* 45, 109–208. doi: 10.1016/S0079-6611(99)00052-X

Hansen, B., Poulsen, T., Húsgarð Larsen, K. M., Hátún, H., Østerhus, S., Darelius, E., et al. (2017). Atlantic water flow through the Faroese Channels. *Ocean Sci.* 13, 873–888. doi: 10.5194/os-13-873-2017

Hátún, H. (2004). *The Faroe Current*. Norway: University of Bergen, 1–113.

Hátún, H., and Chafik, L. (2018). On the recent ambiguity of the North Atlantic subpolar gyre index. *J. Geophys. Res. Ocean.* 2014, 1–5. doi: 10.1029/2018JC014101

Hátún, H., and McClimans, T. A. (2003). *Cont. Shelf Res.* 23, 859–868.

Hátún, H., Sandø, A. B., Drange, H., Hansen, B., and Valdimarsson, H. (2005a). Influence of the Atlantic subpolar gyre on the thermohaline circulation. *Science* 309, 1841–1844. doi: 10.1126/science.1114777

Hátún, H., Sandø, A. B., Drange, H., and Bentsen, M. (2005b). "The Nordic Seas: An Integrated Perspective," in *Geophysical Monograph series*, eds H. Drange, T. Dokken, T. Furevik, R. Gerdes, W. Berger, (American Geophysical Union, Washington, DC, 2005), 158, 239–250.

Hays, G. C. (2003). A review of the adaptive significance and ecosystem consequences of zooplankton diel vertical migrations. *Hydrobiologia* 503, 163–170. doi: 10.1023/B:HYDR.0000008476.23617.b0

Jakobsen, P. K. (2003). Near-surface circulation in the northern North Atlantic as inferred from lagrangian drifters: variability from the mesoscale to interannual. *J. Geophys. Res.* 108:3251. doi: 10.1029/2002JC001554

Köhl, A. (2010). Variable source regions of Denmark Strait and Faroe Bank Channel overflow waters. *Tellus A* 62, 551–568. doi: 10.1111/j.1600-0870.2010.00454.x

Korablev, A. A., Smirnov, A. V., and Baranova, O. K. (2014). *Climatological atlas of the Nordic Seas and Northern North Atlantic. NOAA Atlas NESDIS 77*. Washington, DC: NOAA.

Kristiansen, I., Gaard, E., Hátún, H., Jónasdóttir, S., and Ferreira, A. S. A. (2016). Persistent shift of *Calanus* spp. in the southwestern Norwegian Sea since 2003, linked to ocean climate. *ICES J. Mar. Sci.* 73, 1319–1329. doi: 10.1093/icesjms/fsv222

Kristiansen, I., Hátún, H., Petursdóttir, H., Gislason, A., Broms, C., Melle, W., et al. (2019). Decreased influx of *Calanus* spp. into the south-western Norwegian Sea since 2003. *Deep Sea Res. I Oceanogr. Res. Pap.* 149:103048. doi: 10.1016/j.dsr.2019.05.008

Mork, K. A., and Blindheim, J. (2000). Variations in the Atlantic inflow to the Nordic Seas, 1955-1996. *Deep Res.* 47, 1035–1057. doi: 10.1016/s0967-0637(99)00091-6

Nøst, O. A., and Isachsen, P. E. (2003). The large-scale time-mean ocean circulation in the Nordic Seas and Arctic Ocean estimated from simplified dynamics. *J. Mar. Res.* 61, 175–210. doi: 10.1357/002224003322005069

Ollitrault, M., and Rannou, J. P. (2013). ANDRO: an argo-based deep displacement dataset. *J. Atmos. Ocean. Technol.* 1, 759–788. doi: 10.1175/JTECH-D-12-00073.1

Ollitrault, M., Rannou, J. P., Brion, E., Cabanes, C., Piron, A., Reverdin, G., et al. (2020). *ANDRO: An Argo-Based Deep Displacement Dataset*. London: SEANOE.

Olsen, S. M., Hansen, B., Quadfasel, D., and Østerhus, S. (2008). Observed and modelled stability of overflow across the Greenland–Scotland ridge. *Nature* 455, 519–522. doi: 10.1038/nature07302

Orvik, K. A. (2004). The deepening of the Atlantic water in the Lofoten Basin of the Norwegian Sea, demonstrated by using an active reduced gravity model. *Geophys. Res. Lett.* 31, 1–5. doi: 10.1029/2003GL018687

Pujol, M. I., Faugère, Y., Taburet, G., Dupuy, S., Pelloquin, C., Ablain, M., et al. (2016). DUACS DT2014: the new multi-mission altimeter data set reprocessed over 20 years. *Ocean Sci.* 12, 1067–1090. doi: 10.5194/os-12-1067-2016

Pyper, B. J., and Peterman, R. M. (1998). Comparison of methods to account for autocorrelation in correlation analyses of fish data. *Can. J. Fish. Aquat. Sci.* 55, 2127–2140. doi: 10.1139/cjfas-55-9-2127

Read, J. F., and Pollard, R. T. (1992). Water masses in the region of the Iceland faeroes front. *J. Phys. Oceanogr.* 22, 1365–1378. doi: 10.1175/1520-0485(1992)022<1365:wmitro>2.0.co;2

Richter, K., and Maus, S. (2011). Interannual variability in the hydrography of the Norwegian Atlantic current: frontal versus advective response to atmospheric forcing. *J. Geophys. Res.* 116:C12031. doi: 10.1029/2011JC007311

Richter, K., Segtnan, O. H., and Furevik, T. (2012). Variability of the Atlantic inflow to the Nordic Seas and its causes inferred from observations of sea surface height. *J. Geophys. Res. Ocean.* 117:C04004. doi: 10.1029/2011JC007719

Sandø, A. B., Nilsen, J. E. Ø, Eldevik, T., and Bentsen, M. (2012). Mechanisms for variable North Atlantic-Nordic seas exchanges. *J. Geophys. Res. Ocean.* 117, 1–14. doi: 10.1029/2012JC008177

Semper, S., Pickart, R. S., Våge, K., Larsen, K. M. H., Hátún, H., and Hansen, B. (2020). The Iceland-Faroe Slope Jet: a conduit for dense water toward the Faroe Bank Channel overflow. *Nat. Commun.* 11, 1–10. doi: 10.1038/s41467-020-19049-5

Serra, N., Käse, R. H., Köhl, A., Stammer, D., and Quadfasel, D. (2010). On the low-frequency phase relation between the Denmark Strait and the Faroe-Bank Channel overflows. *Tellus A* 62, 530–550. doi: 10.1111/j.1600-0870.2010.00445.x

Siegismund, F., Johannessen, J., Drange, H., Mork, K. A., and Korablev, A. (2007). Steric height variability in the Nordic Seas. *J. Geophys. Res.* 112:C12010. doi: 10.1029/2007JC004221

Søiland, H., Prater, M. D., and Rossby, T. (2008). Rigid topographic control of currents in the Nordic Seas. *Geophys. Res. Lett.* 35, 1–5. doi: 10.1029/2008GL034846

Voet, G., Quadfasel, D., Mork, K. A., and Søiland, H. (2010). The mid-depth circulation of the Nordic Seas derived from profiling float observations. *Tellus Ser. A Dyn. Meteorol. Oceanogr.* 62, 516–529. doi: 10.1111/j.1600-0870.2010.00444.x

Yang, J., and Pratt, L. J. (2013). On the effective capacity of the dense-water reservoir for the Nordic Seas overflow: some effects of topography and wind stress. *J. Phys. Oceanogr.* 43, 418–431. doi: 10.1175/JPO-D-12-087.1

Conflict of Interest: The authors declare that the research was conducted in the absence of any commercial or financial relationships that could be construed as a potential conflict of interest.

The reviewer RP declared a past co-authorship with several of the authors HH and KMHL to the handling editor.